# Infrastructure monitoring using SAR and multispectral multitemporal images

Datta, U.

U. Datta, "Infrastructure monitoring using SAR and multispectral multitemporal images," Proc. SPIE 11533, Image and Signal Processing for Remote Sensing XXVI, 115330B (20 September 2020); doi: 10.1117/12.2573894

SPIE.

Event: SPIE Remote Sensing, 2020, Online Only

# Infrastructure monitoring using SAR and multispectral multitemporal images

U. Datta
Norwegian Defence Research Establishment (FFI), Instituttveien 20, NO-2007 Kjeller.

## ABSTRACT

The main objective of this study is to investigate suitable approaches to monitor the land infrastructure growth over a period of time using multimodality of remote sensing satellite images. Bi-temporal change detection method is unable to indicate the continuous change occurring over a long period of time and thus to achieve this purpose, synthetic aperture radar (SAR) and multispectral satellite images of same geographical region over a period of 2015 to 2018 are obtained and analyzed. SAR data from Sentinel-1 and multispectral image data from Sentinel-2 and Landsat-8 are used.

Statistical composite hypothesis technique is used for estimating pixel-based change detection. The well-established likelihood ratio test (LRT) statistic is used for determining the pixel-wise change in a series of complex covariance matrices of multilooked polarimetric SAR data. In case of multispectral images, the approach used is to estimate a statistical model from series of multispectral image data over a long period of time, assuming there is no considerable change during that time period and then compare it with the multispectral image data obtained at a later time. The generalized likelihood ratio test (GLRT) is used to detect the target (changed pixel) from probabilistic estimated model of the corresponding background clutter (non-changed pixels). To minimize error due to co-registration, 8- neighborhood pixels around the pixel under test are also considered. There are different challenges in both the cases. SAR images have the advantage of being insensitive to atmospheric and light conditions, but it suffers the presence of speckle phenomenon. In case of multispectral, challenge is to get quite large number of datasets without cloud coverage in region of interest for multivariate distribution modelling. Due to imperfect modelling there will be high probability of false alarm. Co-registration is also an important criterion in multitemporal image analysis.

**Keywords:** Covariance Matrices, Co-registration, LRT, GLRT, SAR, Multispectral, Multitemporal.

## 1. INTRODUCTION

The change detection in remote sensing is the process of identifying differences in the state of an object or a phenomenon by observing it at different points in time [1, 2]. The technique of change detection for remote sensing data has been developed with increase in the spatial resolution of remote sensing images [3]. Change detection involves comparison of the images taken of the same spatial region collected at different points in time, in order to determine what has changed over time. Most of the change detection methods using remote sensing images are spectral based. Remote sensing satellite-based change detection methods are generally using Multispectral, SAR and Hyperspectral data. The most probable change detection is the physical changes corresponding to the changes in material properties, such as reflectance. Even if the images with no change in the scene are taken from same satellites, the change can be due to different reasons like images taken at different time of the day, taken at different seasons, taken from different angles etc. The registration accuracy also affects the change detection, especially in the case of pixel-wise change detection. Most of the methods are bi-temporal pixel-wise change detection method that estimates the change between the corresponding pixels at two different times from the same remote sensing source. But bi-temporal change is unable to indicate the continuous change occurring over a time period. Suitable statistical approaches are considered here for monitoring the various types of infrastructure growth.

urmila.datta@ffi.no; phone +47 6380 7447; www.ffi.no/en

Image and Signal Processing for Remote Sensing XXVI, edited by Lorenzo Bruzzone, Francesca Bovolo
Emanuele Santi, Proc. of SPIE Vol. 11533, 115330B · © 2020 SPIE
CCC code: 0277-786X/20/$21 · doi: 10.1117/12.2573894

The case study in this report is to monitor various continuous changing phenomena like artificial surfaces (built-up land), rail network construction, road construction in and near airport and harbor. SAR images have the advantage of being insensitive to atmospheric and light conditions but it suffers from the presence of speckle phenomenon [4] . The main disadvantage of multispectral image is that a large number image data are always discarded due to cloud coverage. The statistical method is thus not suitable for obtaining a conclusion with small number of datasets. The change detection is estimated in this study using multitemporal SAR data from Sentinel-1 over the year 2015-2018. In earlier publication [5] multispectral remote sensing data sets from Sentinel-2 and Landsat-8 datasets over three years from 2015 to 2018 were used for change detection in the same region of interest. In this paper some results from earlier publication are also shown to compare the different modalities of remote sensing datasets for change detection. The method used in the earlier publication is also explained in brief in section 2.3.

## 2. CHANGE DETECTION METHOD

The change detection method used in SAR datasets are explained in this section. Before explaining the SAR change detection technique, briefly basic SAR polarimetry theory is described as it is relevant for change detection method.

### 2.1 SAR polarimetry

SAR polarimetry explores the target properties from the behaviors of backscattered polarized electromagnetic waves such as HH (Horizontal-Horizontal), HV (Horizontal-Vertical), VH (Vertical-Horizontal), and VV (Vertical-Vertical). In the monostatic backscattering case, where the transmitting and receiving antennas are placed at the same location [4]. The complex scattering vector $S$ , of dimension $d = 3$ is expressed as:

$$S = [S_{hh}, \sqrt{2}S_{hv}, S_{vv}]^T \tag{1}$$

The elements of $S$ represent the complex backscattering coefficients of the polarimetric channels. $S_{hh}$ and $S_{vv}$ are co-polar and $S_{hv}$ and $S_{vh}$ are named as cross-polar scattering components. Multilook polarimetric SAR processing requires averaging several independent $L$ -look covariance matrices. The $L$ -look covariance matrix has appropriate representation of the backscattered signal of the covariance matrix expressed in a single matrix as:

$$\langle C \rangle = \frac{1}{L}\sum_{l=1}^{L} S_l * S_l^T \tag{2}$$

Where, $\langle \bullet \rangle$ denotes ensemble averaging and $^*$ denotes complex conjugation. In Sentinel-1 case the data is dual polarization $S_{vv}$ and $S_{vh}$ . The reciprocity which normally applies to natural targets gives $S_{vh} = S_{hv}$ [6]. The cross- polarized components such as $\langle S_{vh} S_{vv}^* \rangle$ and $\langle S_{vv} S_{vh}^* \rangle$ often have little information. For randomly distributed targets with azimuthal symmetry, the elements are zero [7]. Therefore, the covariance matrix expression for Sentinel-1 data becomes:

$$\langle C \rangle_{dual} = \begin{bmatrix} \langle S_{vv} S_{vv}^* \rangle & 0 \\ 0 & \langle S_{vh} S_{vh}^* \rangle \end{bmatrix} \tag{3}$$

For the multilook conditions, each pixel feature of SAR images is modeled as the covariance complex matrix [8] obeying Wishart distribution. For $p \times p$ Hermitian matrix it is expressed as:

$$X \in W(p, n, \Sigma_x) \tag{4}$$

$\sum_x$ is the sample covariance and $n$ is the number of looks. The probability distribution function of Wishart distribution is given by [9]:

$$w(x) = \frac{1}{\Gamma_p(n)\left|\sum_x\right|^n}\left|x\right|^{n-p}\exp(-tr\left[\sum_x{}^{-1}x\right] \tag{5}$$

$\Gamma_p(n) = \pi^{p(p-1)/2}\prod_{j=1}^{p}\Gamma(n-j+1)$ is the gamma function and $\left|\sum_x\right|$ and $\left|x\right|$ are the determinants of $\Sigma_x$ and $x$ respectively. The trace of the matrix is the total energy of the received signal and is generally called span.

### 2.2 LRT for change detection

For two temporal SAR images with independent Wishart distribution $X \in W_c(p,n,\sum_x)$ and $Y \in W_c(p,m,\sum_y)$, the composite hypothesis test is the statistic test of $H_0$, i.e. null hypothesis against alternative $H_1$ i.e. change is given by

$$H_0 : \sum_x = \sum_y \text{ against } H_{1,} : \sum_x \neq \sum_y \tag{6}$$

Likelihood ratio test statistic becomes [10]:

$$Q = \frac{L(\hat{\Sigma})}{L_x(\hat{\Sigma}_x)L_y(\hat{\Sigma}_y)} \tag{7}$$

Where, $L_x(\hat{\Sigma}_x) = \frac{1}{\Gamma_p(n)}\left|\frac{1}{n}X\right|^{-n}\left|X\right|^{n-p}\exp\{-ntrI\}$ and $L_y(\hat{\Sigma}_y)$ has the similar expression as $L_x(\hat{\Sigma}_x)$. The numerator of $Q$ can also be expressed as:

$$L(\hat{\Sigma}) = \frac{1}{\Gamma_p(n)\Gamma_p(m)}\left|\frac{1}{n+m}(X+Y)\right|^{-(n+m)}\left|X\right|^{n-p}\left|Y\right|^{m-p}\exp\{-(n+m)trI\} \tag{8}$$

This leads to the desired likelihood ratio test as equation(7):

$$Q = \frac{(n+m)^{p(n+m)}\left|X\right|^n\left|Y\right|^m}{n^{pn}m^{pm}\left|X+Y\right|^{n+m}} \tag{9}$$

In case of change detection the number of looks for two images are same i.e. $n = m$ and thus log likelihood ratio of equation (9) becomes:

$$\ln Q = n(2p\ln 2 + \ln\left|X\right| + \ln\left|Y\right| - 2\ln\left|X+Y\right|) \tag{10}$$

If the detected value of $-2\ln Q$ is $z = -2\ln q_{obs}$, then the probability [11] of finding a smaller value of $-2\ln Q$ is given by:

$$P\{-2\ln Q \leq z\} \cong P\{\chi^2(p^2) \leq z\} \tag{11}$$

The number of looks in practical case is a small quantity for typical SAR images. Auxiliary variables $\omega_2$ and $\rho$ are introduced in some cases for better approximation of probability [9].

In case of multitemporal datasets the test statistic is known as Omnibus likelihood ratio test statistic [12]. It is a factorization of the test statistic for change detection of a time-series of multilook polarimetric SAR data. The test statistic evaluates if there is a change occurred in a temporal datasets $t(t_1 < t_j \le t_k)$. If the above test shows that we cannot reject the hypothesis of equality, no change has occurred over the time span covered by the data. If we can reject the hypothesis, change has occurred at some point in time. The likelihood ratio test statistic $R_j$ for hypothesis testing for first *j* variance of complex covariance matrices equality is expressed as:

$$H_{0,j} : \sum_j = \sum_1 \text{ against } H_{1,j} : \sum_j \neq \sum_1$$

$$R_j = \left\{ \frac{j^{jp}}{(j-1)^{(j-1)p}} \frac{\left|X_1 + X_2 + X_3 + ... + X_{j-1}\right|^{j-1} \left|X_j\right|}{\left|X_1 + X_2 + X_3 + ... + X_{j-1} + X_j\right|^{j}} \right\}^n \tag{12}$$

The log likelihood ratio statistics becomes:

$$\ln R_j = n\{p(j \ln j - (j-1)\ln(j-1)) + (j-1)\ln\left|\sum_{i=1}^{j-1} X_i\right| + \ln\left|X_j\right| - j\ln\left|\sum_{i=1}^{j} X_i\right|\} \tag{13}$$

This constitutes a factorization of $Q$ where:

$$Q = \prod_{j=2}^{k} R_j \text{ or } \ln Q = \sum_{j=2}^{k} \ln R_j \tag{14}$$

If $H_0$ is true, then $R_j$ are independent. A simple expression of probability of finding a smaller value of $-2\ln R_j$ is:

$$P\{-2\ln R_j \le z_j\} \simeq P\{\chi^2(p^2) \le z_j\} \tag{15}$$

### 2.3 GLRT for change detection

GLRT method used in multitemporal multispectral images is explained in detail in earlier publication [5].The target detection from background clutter [13,14] is a well-established method. The GLRT detection algorithm is defined as a collection of decision rules [15].

$$d_{GLRT}(x:\lambda) = \frac{\underset{\theta_T \in \Theta_T}{\text{Max}}\, p_T(x:\theta_T)}{\underset{\theta_B \in \Theta_B}{\text{Max}}\, p_B(x:\theta_B)} - \lambda \tag{16}$$

Where, $p_T(x:\theta_T)$ the probability distribution of target pixels to be determined as changed or unchanged and $p_B(x:\theta_B)$ is the unchanged pixel distribution modelled as background pixels. $\lambda$ is an adjustable threshold value depending upon educated guess.

Alternative way of writing the same expression is:

$$d_{GLRT} = \underset{T}{Max}(\underset{B}{Min}[d(x:\theta_T, \theta_B, \lambda)]) \tag{17}$$

The general procedure of processing framework for analysis of datasets of Sentinel-2 and Landsat 8 are shown in the form

of flow chart in figure1. It is used for estimating pixel-based change detection in a defined region over a period of time. The target pixel may not be the corresponding background pixel (due to co-registration error) but may also be any of the 8-neighbourhood pixels. Therefore, all these 9 pixels are considered, taking due account of possible co-registration error, for change detection calculation as shown in figure2.

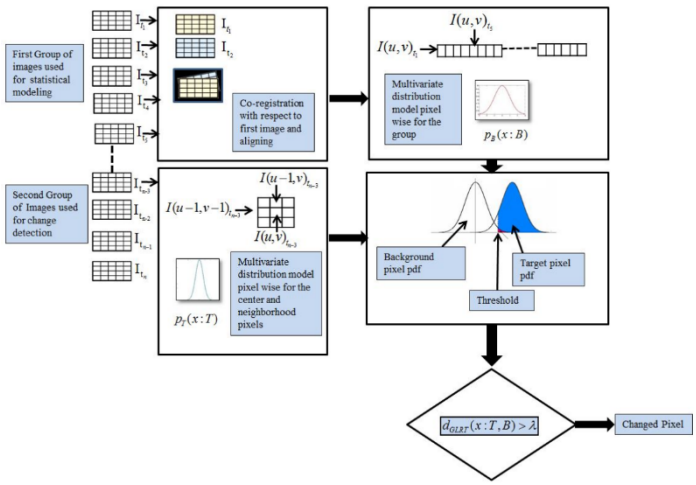


Figure1 Processing framework of Sentinel-2 and Landsat-8 images

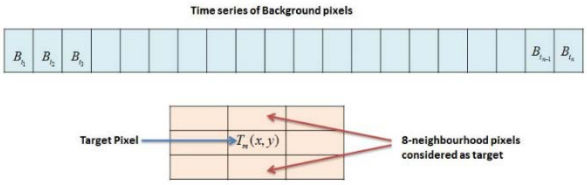


Figure2 Time series of background pixels and 8-neigbourhood of target pixels

## 3. DATASETS AND PREPROCESSING

The SAR datasets of Sentinel-1 Level-1 GRD (Ground Range Detected) data are obtained from Copernicus Open Access Hub [16]. The multispectral datasets of Sentinel-2 are also obtained from the same open source. The Landsat-8 products are also obtained at free of cost from Earth Explorer data portal [17].


Figure 3 The picture of Stockholm Norvik Hamn taken from google earth. The figure (a) is taken in 2015 and the figure (b) is taken in 2018. Rectangular Square with yellow borderline is the area of interest (AOI).

The area called Stockholm Norvik Hamn is selected for analysis. It is Sweden's harbor area. In this area, there is an ongoing project for building the harbor for rolling goods and containers at Norvikudden, outside Nynashamn. In addition to the harbor, ~~a~~ railway was also being connected to Nynasrailway network, and a construction group was building a logistics and business park adjacent to the harbor. In figure 3 the first picture is taken in the year 2015 and the second in 2018. Visual inspection shows the change due to infrastructure growth. So the conclusion is that it is a right choice of area for analysis. The Sentinel-1 GRD scene is composed of approximate square pixels. The multilook processing results the final product with reduced speckle. The final product is the detected amplitude, but the phase information is lost. Before data analysis it is preprocessed using the SNAP software for further reduction of speckle noise and terrain correction [18]. The total preprocessing is divided into six steps as shown in figure 4 .

In case of multispectral images the datasets are downloaded for Sentinel-1 and Landsat-8 by defining same area of interest as Sentinel-1 and defining a certain period of time and percentage of cloud coverage. The RGB (red-green-blue) quick look view of the image is produced by combining band 2, 3 and 4 in case of Sentinel-2. Quick look view helped to select the data sets that can be used for further processing. Some of the datasets, depending on time of the year, has more cloud coverage. Especially if the area of interest is mostly covered by clouds then it has to be rejected for processing. The bands with 10m resolution in Sentinel-2 are preprocessed to decrease to 20m resolution to have all spectral bands taken to be under consideration for processing having same spatial resolution. In case of Landsat-8 all bands considered are of 30m resolution.

Change detection is a major application in remote sensing. It aims at detecting areas of an image that have changed between two given dates or multiple dates. The co-registration is very important preprocessing step that aims to compute the images on a common spatial grid. The pixel-based change detection method has special requirement of co-registration accuracy. In multispectral datasets FFT co-registration approach [19] was used to estimate registration error between the satellite images from the same Sentinel-2 tiles and Landsat-8 products. This technique has registration accuracy in subpixel order. In case of SAR images of Sentinel-1 data another successful co-registration method is used based on eFOLKI (Extended Flow Optical Lucas–Kanade Iterative estimation technique). This method is further developed and applied for co-registration of SAR-SAR, SAR-LIDAR and SAR-optical images [20]. The method is known as GeFolki (Geoscience Extended Flow Optical Lucas–Kanade Iterative).

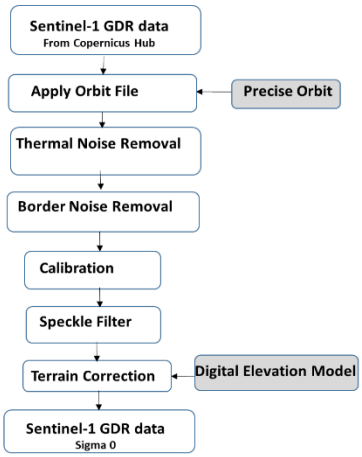


Figure 4 Sentinel-1 GRD preprocessing Workflow used in snap software.

Some results are shown here using GeFolki co-registration technique. Figure 5 is the coregistered image of backscattered VV and VH polarized data of 9th June, 2015 and 25th November, 2017, 26th December, 2018 respectively. The two images of different dates are overlaid and the color difference shows some indication of change. Figure 6 is the co-registered image of Sentinel-1 SAR and Sentinel-2 multispectral datasets taken within two days of interval. Figure 6a) shows subsets of both multispectral and SAR projected on Earth's google map. Figure 6 b) is the RGB image of Sentinel-1 VV, Sentinel-2 Red and Blue band co-located. Figure 6 c) of the same figure is the coregistered image of backscattered VV of Sentinel-1 and Red band of Sentinel-2.

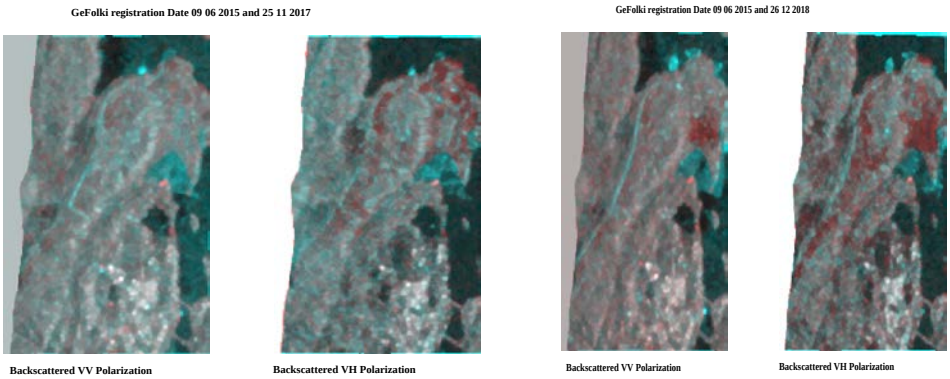


Figure 5 Co-registration of Sentinel 1 GRD data sets between 9th June,2015 & 25th November, 2017 and between 9th June,2015 & 26th December,2018 respectively.

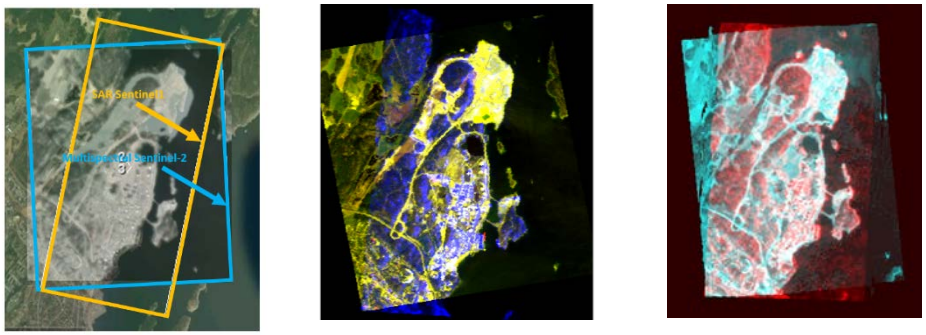


a b c

Figure 6 a) Sentinel-2 data on 27th May, 2017 and 29th May, 2017 SAR Sentinel-1 data on Google earth geo-located b) RGB image of Sentinel-1 VV, Sentinel-2 Red and Blue band co-located, c) Co-registration of Backscattered VV polarized SAR image taken on 28th March and Red band of Multispectral image taken on 25th March, 2017.

## 4. RESULTS AND ANALYSIS

The main objective of this change detection is to monitor the change in infrastructure over three years of time. The change is estimated pixel-wise. For preliminary analysis of change detection of SAR data the scatter plots of VV and VH data is analyzed between several dates shown in figure 7.

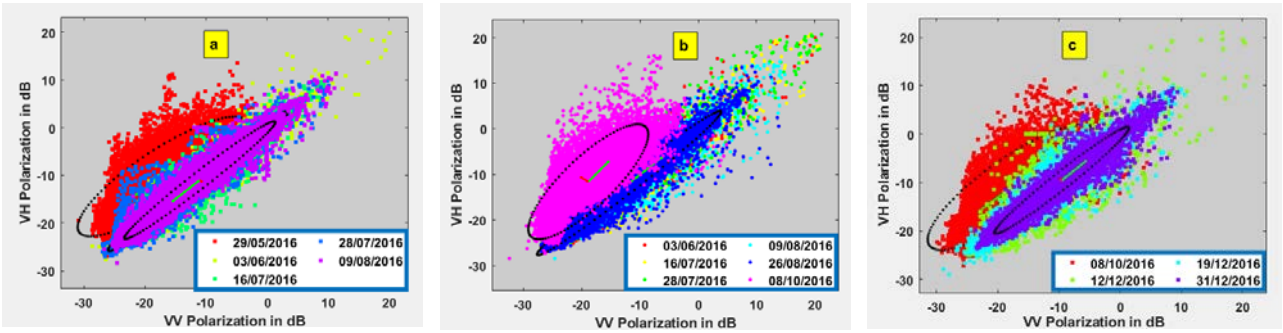


Figure 7 Scatter plots of VV verses VH in the year 2016

The spread of VV and VH when compared with different datasets gives the idea of when the change has happened. In figure 7 , the plot marked a) shows that the datasets on 29th May, 2016 is different from other four datasets from June to August, 2016, the plot marked b) and c) indicates that again on 8th October, 2016 there may have been some change than the datasets in earlier dates and later dates of 2016. Figure 8 shows the preliminary indication of when change happened over the year of 2017 datasets. The plot marked a) shows that the change may have happened on 13th March, 2017. The plot marked b) in the figure shows that there is a change on 11th April, 2017 than other dates in same plot. Similar types of behavior shown in the plot marked c) such as the change on 30th April, 2017 and then no noticeable change for other later datasets of 2017. In case of multispectral data scatterplots also shows similar type indications of change. Figure 9 shows the comparison of two dimensional scatter plots of Red and NIR (near infra-red) band of same pixel region at different dates of Sentinel-2 image. The first figure explains that the spread along red band is much more in on 29th October, 2016 than the other dates in the same year and also the second figure indicates same behavior on last two dates in 2017. It indicates that change from green vegetation to build-up land.

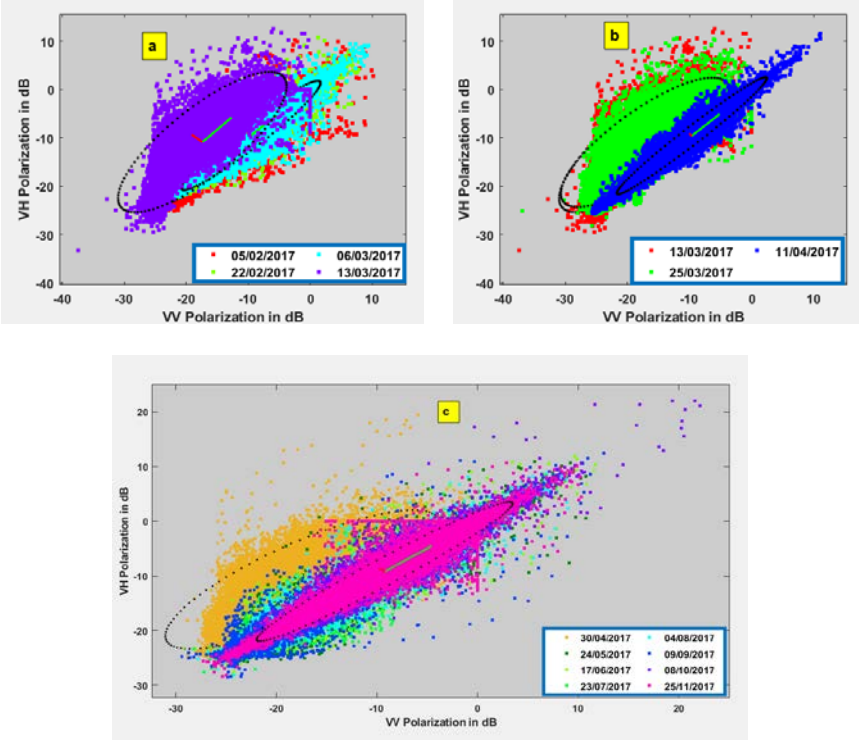


Figure 8 Scatter plots of VV verses VH in the year 2017

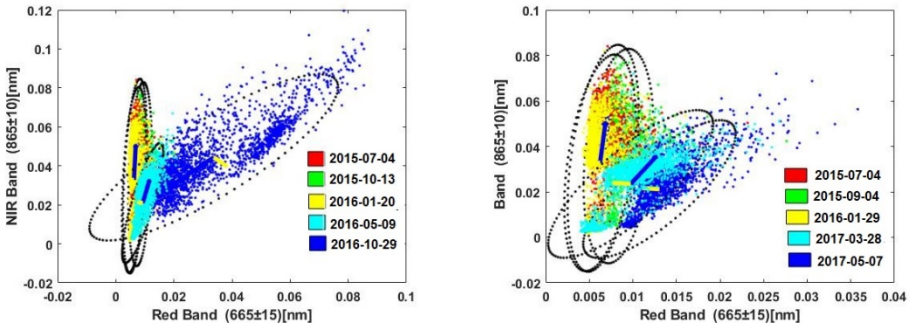


Figure 9 Comparison of two dimensional scatter plots of same pixel regions but from different dates of Sentinel-2 Image.

Figure 10 is changed pixel plot in different years of the datasets of Sentinel-2. The color bar corresponds to the dates of the datasets. The color code corresponds to changed pixels in different dates of each year plotted in same image with zero corresponding to the base date i.e. 9th June, 2015. All comparisons shown in the figure 10 are made with respect to the base date. It is obvious from the plot that the changed pixels are more in 2017 and 2018 than in the year 2015 or during the first half of the year of 2016. It is pixel based change analysis considering a threshold value of probability. If the probability of change is greater than the threshold then it is considered that the pixel is changed. Figure 11 is the plot of frequency i.e. how many times each pixel is changed during the whole year datasets. The results clearly show more activities during 2017 and 2018.

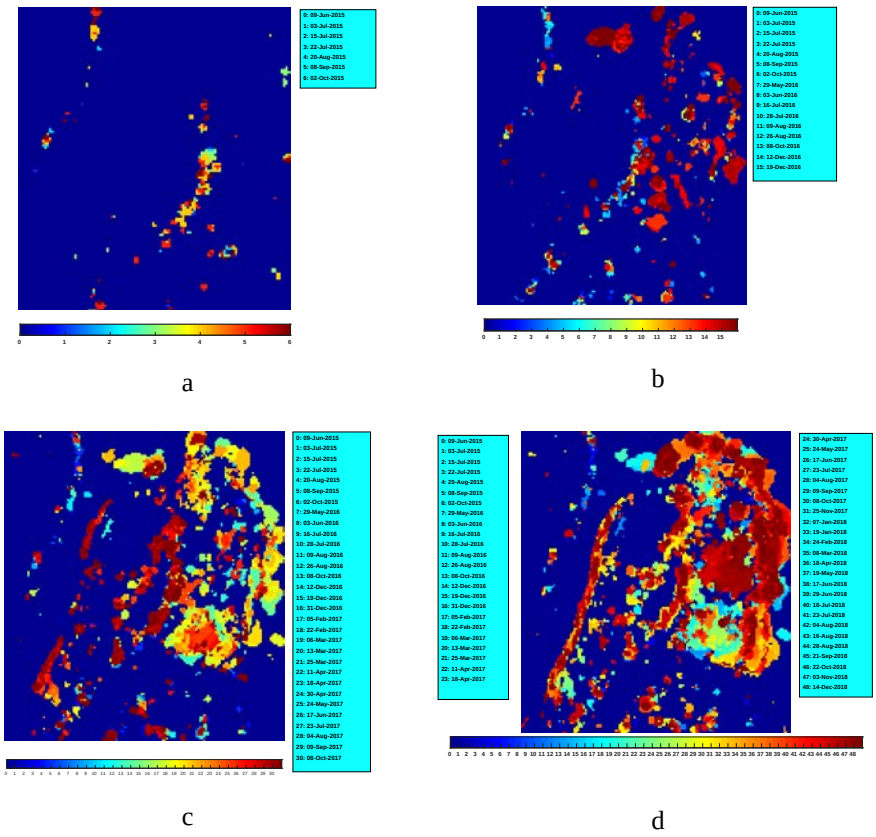

a b c d

Figure 10 Plot of changed pixels in the area of interest a) Year 2015 with 6 datasets, b) Year 2015-2016 with 15 datasets, c) Year 2015-2017 with 31 datasets, d) Year 2015-2018 with 49 datasets. Color indicates pixel changes in particular dates.

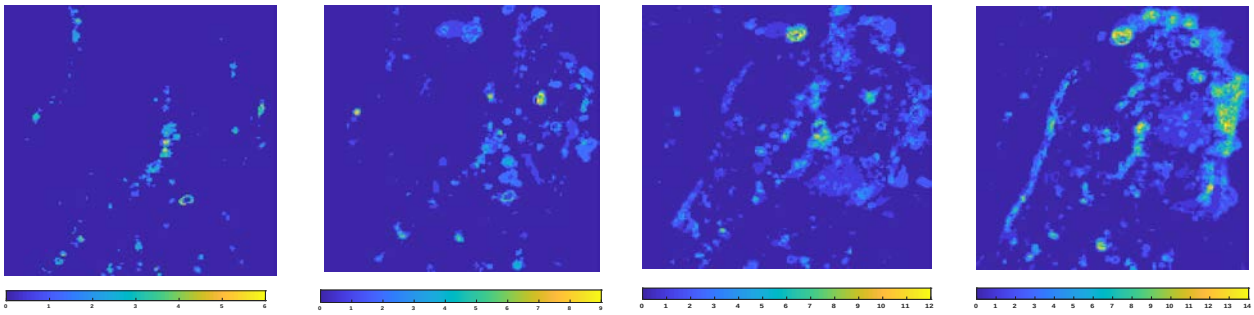

a b c d

Figure 11 The frequency of each pixel changed over the whole year's datasets. a) Year 2015 b) 2016 c) 2017 d) 2018

Figure 12 is the GLRT result of changed pixels plot from Sentinel-2 and Landsat-8 datasets during different dates of the year 2017. The comparison with results of Sentinel-1and Landsat-8 shows clearly the change detection is in the same region of interest. The fourth image in part b) of figure 12 has a part covered with clouds and it is not at all of good quality for processing. In spite of that, it shows some detected changed pixels over the region of interest selected, shown by red circles. Lastly figure 13 is an example of Sentinel-2 and Landsat-8 image at same year and approximately within a gap of four months. Comparison between them visually shows that some detected changed pixels are nearly over the same area.


a b

Figure 12 The changed pixels shown as red squares in different dates as a result of GLRT test in a) Sentinel-2 datasets, b) Landset-8 datasets.


Figure 13 The detected changed pixels shown both in Sentinel-2 and Landsat-8 in approximately four months gap.

## 5. CONCLUSION

The objective in this study is to investigate suitable approaches to monitor the land infrastructure growth over a period of time using multimodality of remote sensing satellite images. In this study SAR and multispectral satellite datasets are considered to monitor the same geographical area of interest over a period of 2015 to 2018. Statistical composite hypothesis technique with two different approaches are used in this study.

SAR images have the advantages over multispectral of being insensitive to atmospheric and light conditions, but suffers the presence of speckle phenomenon. Thus preprocessing step is important before analyzing SAR to reduce further speckle noise and to get a terrain corrected dataset. In case of acquiring multispectral datasets there is great a challenge to get quite large number of datasets without cloud coverage. The imperfect modelling causes high probability of false alarm. Co-registration is also an important criterion for both SAR and multispectral multitemporal image analysis.

Overall conclusion that can be drawn from this work is that the statistical methods used for both SAR and multispectral datasets to monitor infrastructure growth has given some promising results. The comparison of SAR and multispectral data analysis has given a preliminary idea for multimodal approach of studies. It can be developed further to study direct fusion of multimodalities of remote sensing satellite images. A possible approach can be principal component analysis after direct fusion of two modalities.

## REFERENCES


[1] Kotkar, S. R. and Jadhav, B. D., "Analysis of various change detection techniques using satellite images," International Conference on Information Processing (ICIP), 664-668 (2015).

[2] Hegazy, I.R. and Kaloop, M.R., "Monitoring urban growth and land use change detection with GIS and remote sensing techniques in Daqahlia governorate Egypt," International Journal of Sustainable Built Environment 4(1), 117-124 ( 2015).

[3] Xiao, P.; Zhang, X.; Wang, D.; Yuan, M.; Feng, X. and Kelly, M.; "Change detection of built-up land: A framework of combining pixel-based detection and object-based recognition," ISPRS Journal of Phogrammetry and Remote Sensing (119), 402-414 ( 2016).

[4] Pottier, J. S. L. E., [Polarimetric Radar Imaging: From Basics to Applications], Boca, Raton, USA: CRC Press, Taylor & Francis Group (2009).

[5] Datta, U.; "Infrastructure Change Monitoring Using Multitemporal Multispectral Satellite Images," International Journal of Civil and Architectural Engineering 14(5), 155-160 (2020).

[6] Lay, F.T; Charles E., Ed. [Radar polarimetry for geoscience applications], Norwood, MA, Artech House Inc (1990).

[7] Esmaeilzade, M.; Jelani, F.; Amini, J.; "Using Covariance Matrix For Change Detection Of Polarimetric SAR Data," The International Archives of the Photogrammetry, Remote Sensing and Spatial Information Sciences (XLII-4/W4), 69-76 (2017)

[8] Kersten, P. R.; Lee, J. S.; and Ainsworth, T. L.; "Unsupervised classification of polarimetric synthetic aperture Radar images using fuzzy clustering and EM clustering," IEEE Transactions on Geoscience and Remote Sensing 43(3), 519-527(2005).

[9] Conradsen, K.; Nielsen, A. A.; Schou, J. and Skriver, H.; "A test statistic in the complex Wishart distribution and its application to change detection in polarimetric SAR data," IEEE Transactions on Geoscience and Remote Sensing 41(1), 4-19 (2003)

[10] Conradsen, K.; Nielsen, A. A.; Schou, J. and Skriver, H.; "Change detection in polarimetric SAR data and the complex Wishart distribution," IEEE 2001 International Geoscience and Remote Sensing Symposium 6, 2628-2630 (2001).

[11] Canty, M.J.; [Image Analysis, Classification and Change Detection in Remote Sensing: With Algorithms for Python], CRC Press, 508 (2019).

[12] Nielsen, A. A; Conradsen, K and Skriver, H.; "Omnibus test for change detection in a time sequence of polarimetric SAR data," IEEE International Geoscience and Remote Sensing Symposium (IGARSS), 3398-3401(2016).

[13] Schaum, A.; "Theoretical foundation of NRL spectral target detection algorithm," Applied Optics 54(31), 288-296 (2015).

[14] Schaum, A.; "Clairvoyant fusion: a new methodology for designing robust detection algorithms," Proc. SPIE 10004, Image and Signal Processing for Remote Sensing XXII, 2016.

[15] Schaum, A.; "CFAR fusion:A replacement for generalized likelyhood ratio test for Neyman-Pearson problems," IEEE Computer Society, 1-6 (2011).

[16] Copernicus Open Access Hub [Online], https://scihub.copernicus.eu/dhus/#/home .

[17] USGS Earth Explorer data portal, https://earthexplorer.usgs.gov/.

[18] Filipponi, F.; "Sentinel-1 GRD Preprocessing Workflow," The 3rd International Electronic Conference on Remote Sensing 3(2019)

[19] Guizar-Sicairos, M.; Thurman, S. T. and Fienup, J.R.; "Efficient subpixel image registration algorithms," OPTICS LETTERS, 33(2), 156-158(2008).

[20] Plyer, A.; Colin-Koeniguer, E. and Weissgerber, F.; "A New Co-registration Algorithm for Recent Applications on Urban SAR Images," IEEE Geoscience and Remote Sensing Letters, 12 (11), 2198-2202(2015).